SLAC-PUB-14351
January 2011

ANALYSIS AND MITIGATION OF X-RAY HAZARD GENERATED FROM HIGH INTENSITY LASER-TARGET INTERACTIONS [1]

Paper # 503

R. Qiu, J. C. Liu, A. A. Prinz, S. H. Rokni, M. Woods and Z. Xia

SLAC National Accelerator Laboratory,
2575 Sand Hill Rd., Menlo Park, CA 94025

Abstract

Interaction of a high intensity laser with matter may generate an ionizing radiation hazard. Very limited studies have been made, however, on the laser-induced radiation protection issue. This work reviews available literature on the physics and characteristics of laser-induced X-ray hazards. Important aspects include the laser-to-electron energy conversion efficiency, electron angular distribution, electron energy spectrum and effective temperature, and bremsstrahlung production of X-rays in the target. The possible X-ray dose rates for several femtosecond Ti:sapphire laser systems used at SLAC, including the short pulse laser system for the Matter in Extreme Conditions Instrument (peak power 4 TW and peak intensity 2.4×10^{18} W/cm^2) were analysed. A graded approach to mitigate the laser-induced X-ray hazard with a combination of engineered and administrative controls is also proposed.

1. Introduction

A plasma is produced when a pulsed laser beam is focused on a solid target at peak intensities of 10^{12} W/cm^2 or higher [1]. Laser-plasma interactions subsequently accelerate electrons to high energies (10's to 1000's of keV), thereby creating "hot" electrons. These hot electrons will interact with ions in the target and generate bremsstrahlung X-rays, which become an ionizing radiation source [2,3,4,5,6,7]. The hot electrons have a Maxwellian-like energy distribution characterized by an electron temperature, *T*.

If the X-ray energy is high enough to exceed the threshold of photonuclear reactions, these reactions can take place in the target or walls of the experimental target chamber leading to the generation of neutrons [8]. Energetic protons can also be produced when thin metallic targets are irradiated by ultra-intense short laser pulses due to the electrostatic acceleration of protons at the target rear (non-irradiated) surface [9].

Measurements show that significant amounts of radiation can be generated from high intensity laser-target interactions [8, 10 , 11]. Therefore, it is necessary to analyze and evaluate the X-ray hazard when a high intensity laser is hitting a target in vacuum. However, very limited studies have been made on the laser-induced ionizing radiation hazard and protection issues.

At laser intensities below ~10^{19} W/cm^2, X-ray radiation is the main ionizing radiation of concern. The radiation source term depends on the X-ray flux and energy spectrum and is characterized by the dose rate per laser shot (given in mrem/J) at a given distance

[1] Contributed to the 2011 International Laser Safety Conference, San Jose, CA; http://www.laserinstitute.org/conferences/ilsc/conference

Work supported by the U.S. Department of Energy under contract number DE-AC02-76SF00515.

from the target. We have reviewed available literature on the physics and characteristics of laser-induced X-rays and have developed a hazard analysis methodology to estimate potential radiation spectrum and dose.

We present preliminary radiation analysis results for several scenarios that utilize femtosecond Ti:sapphire (TiS) laser beams focused to small spot sizes on a solid target in vacuum. The absorption and heating mechanism is different depending on the laser system parameters (laser energy, pulse width, spot size, repetition rate, etc.) and target conditions (material, phase, geometry, etc.). Although a lot of studies have been carried out to understand the physics of the laser-plasma interaction [2, 12, 13, 14], as stated by S. C. Wilks [2], new theoretical and experimental results are constantly refining and adding to the understanding of ultra-short ultra-intense laser–matter interactions.

In this study laser systems with intensities between 10^{14} and 10^{20} W/cm^2 were analyzed. One particular example is the laser system planned for the Matter in Extreme Conditions Instrument (MECI) at SLAC [15]. MECI is an X-ray instrument that will be able to create high energy density matter and measure its physical properties. It is located at Hutch 6 of the Linac Coherent Light Source (LCLS), the world's first hard X-ray free electron laser (FEL). It will utilize either the LCLS FEL beam and/or one or more optical lasers focused onto the target to create and probe matter in extreme conditions [16]. The hutch shielding is mainly designed to mitigate radiation hazards from FEL operation, but the shielding for potential X-ray radiation from laser-target interactions with the high intensity optical lasers is also evaluated.

Figure 1 shows the configuration and system components of the MECI laser system. It is a TiS laser with a regenerative amplifier, a subsequent multi-pass amplifier and a vacuum pulse compressor. It operates at a wavelength of 800 nm, with capability to provide 150 mJ pulse energy, 40 fs pulse width and 4 TW peak power. When focused to a spot size of 10 μm (1/e^2 radius), the peak intensity is calculated to be 2.4x10^{18} W/cm^2. The laser system may later be upgraded to have a much higher peak power of 100 TW with intensity of 6.4x10^{19} W/cm^2.

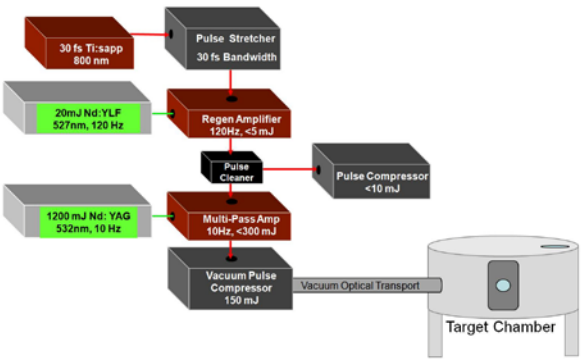

Figure 1. Configuration for the MECI laser system

2. Electron source term and the characteristics

Three key factors affecting the electron source term are evaluated: i) the laser to electron energy converhsion efficiency, ii) electron spectrum and electron temperature, and iii) angular distribution of hot electrons.

2.1 Laser to electron energy conversion efficiency

The electron yield is characterized by the laser-to-electron energy conversion efficiency, which represents the fraction of the laser energy on the target converted to the total energy of hot electrons. Many experiments show that 10-50% of laser energy is converted to hot electrons at incident intensities of 10^{18} to 10^{20} W/cm^2 [17,18,19,20,21,22], though the data are not always conclusive and consistent. The paper [17], which has laser intensities similar to the MECI laser, gives conversion efficiencies of 12%, 18% and 50% at 2x10^{18}, 10^{19} and 3x10^{20} W/cm^2, respectively, from solid targets. On the other hand, T. Guo [5] reports that the laser to electron energy conversion efficiency is approximately 30% for laser intensities between 5x10^{17} and 5x10^{18} W/cm^2. A laser to electron energy conversion efficiency of 33% was used in the dose and shielding calculation for the National Ignition Facility [23]. In this study, a conservative conversion efficiency of 30% for laser intensity below 10^{19} W/cm^2 and 50% above 10^{19} W/cm^2 was used for absolute dose calculations (see section 3.2).

2.2 Electron spectrum and electron temperature

Three slightly different distributions (Boltzmann distribution [24, 25], Maxwellian distribution [26, 27], and Relativistic Maxwellian distribution [6, 9, 28]) have been used to describe the hot electron spectrum generated from a high intensity laser hitting a solid target. Whichever formula is used, the exponentially decreasing feature is well known and an effective

electron temperature, T, is the key parameter to characterize the exponentially decreasing slope of the electron spectrum. The electron spectrum studies at Lawrence Livermore National Laboratory (LLNL) [29] show that the hot electron temperature depends strongly on the laser intensity and wavelength but not on the atomic number of the target. For solid targets, the electron temperature is usually defined as a function of the normalized laser intensity ($I\lambda^2$), which is the product of the laser intensity, I (W/cm^2), and the square of the laser wavelength, λ (μm).

For normalized laser intensities in the range 10^{12} W/cm^{2}μm^2 < $I\lambda^2$ < 10^{17} W/cm^{2}μm^2, Ref. [2] stated that inverse bremsstrahlung and resonance absorption are the dominant absorption mechanisms, with electron temperature expected to scale as $(I\lambda^2)^{1/3}$. An experimental result of the temperature scaling is described in reference [30], which gives

$$T \approx 6\times10^{-5}\left[I\lambda^2\right]^{1/3} \quad (1)$$

where T is the electron temperature in keV, I is the laser intensity in W/cm^2, and λ is the laser wavelength in μm.

For very high normalized laser intensities, $I\lambda^2 > 10^{18}$ W/cm^{2}μm^2, relativistic J x B Heating becomes the dominant absorption mechanism. The electron temperature can be estimated by Equation 2 based on the ponderomotive force theory,

$$T = M_e \times (-1.0 + \sqrt{1.0 + I\lambda^2 / 1.37\times10^{18}}) \quad (2)$$

where M_e is the electron rest mass (0.511 MeV) [9,26].

Reference [31] compared experiment results at the Rutherford Appleton Laboratory (RAL) Vulcan petawatt laser facility and the Callisto Ti:sapphire laser at the Jupiter laser facility at LLNL with a calculation based on the ponderomotive theory. Even though the experiment results show electron temperature increasing as $(I\lambda^2)^{0.34}$, they were also observed to agree with the estimate using Equation 2 from ponderomotive scaling to within a factor of two for normalized laser intensities in the range 10^{18} W/cm^{2}μm^2 < $I\lambda^2$ < 10^{20} W/cm^{2}μm^2.

Results for the electron temperature using Equations 1 and 2 and experiment results summarized in [29] are shown in Figure 2. Electron temperature estimates based on Equations 1 and 2 are observed to coincide when $I\lambda^2$ = 1.6x10^{17} W/cm^{2}μm^2. In this study we decided to use Equation 1 to estimate the electron temperature when $I\lambda^2$<1.6x10^{17} W/cm^{2}μm^2, while Equation 2 was used when $I\lambda^2 \geq$ 1.6x10^{17} W/cm^{2}μm^2.

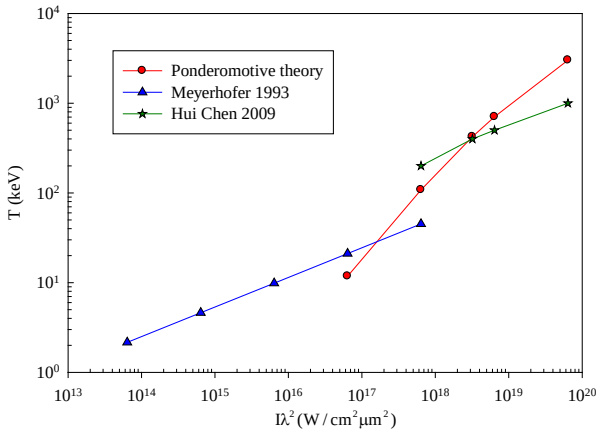

Figure 2. Electron temperature, T, versus $I\lambda^2$.

2.3 Angular distribution

Reference [32] has measured the angular distributions of hot electrons with very thin thermoluminescent dosimeters with a resolution of 10 degrees for 45-degree incidence onto a target at laser intensities of 10^{18}-10^{20} W/cm^2. At an intensity of 8x10^{17} W/cm^2, most of the hot electrons are at lower energies and the electron dose rate peaks at the target's front side, likely due to target self-shielding. At an intensity of 2x10^{19} W/cm^2, the dose rate component behind the target increases. As the intensity reaches 8x10^{19} W/cm^2, hot electrons are more energetic and the electron dose rate peaks at the back side with additional peaks in the laser direction.

These results show that the angular distribution of hot electrons is not isotropic (but is not very anisotropic either) due to the energies of hot electrons and the target self-shielding. In this study, the X-ray source is assumed to be isotropic. This assumption probably results in an uncertainty factor of 2-4 in the dose rate estimate, depending on the laser intensity and target conditions.

3. X-ray spectrum and dose

Using the electron source term discussed in section 2, the X-ray dose can be calculated from the bremsstrahlung process in a target, and using the estimated conversion efficiency of laser energy to electron energy and the electron temperature.

3.1 X-ray spectrum

Studies have shown that the bremsstrahlung X-ray spectrum can be expressed as [4, 33]:

$$N_p(E_p) = C\frac{1}{E_p}\exp(-\frac{E_p}{T}) \qquad (3)$$

where E_p is the photon energy, T is the electron temperature, and C is a constant.

C should satisfy that the integration of the energy of all the photons equates to the product of the laser pulse energy and the laser energy to X-ray energy conversion efficiency. Therefore C is dependent on the electron temperature, the laser pulse energy, and the laser to X-ray energy conversion efficiency. The laser to X-ray energy conversion efficiency is determined by two processes: conversion of laser energy to the energy of hot electrons; and conversion of the energy of hot electrons to bremsstrahlung. Note that isotropic emission of the X-ray is assumed in the formula.

This X-ray spectrum formula is consistent with the electron spectra described in section 2.2, when a bremsstrahlung yield spectrum of E_p^{-1} or E_p^{-2} is used [34]. M. H. Key et al. [18] also mentioned that a Maxwellian electron energy distribution gives an $e^{-Ep/T}$ spectral shape of the bremsstrahlung. Therefore, Equation 3 was used to describe the X-ray source spectrum in the shielding attenuation calculations in sections 3.3 and 3.4.

3.2 Calculations of X-ray dose

Y. Hayashi et al. derived Equation 4 to estimate the 0-degree photon dose generated from the interaction of a short pulse high power laser and a solid target [11],

$$H_x \approx 6.0\times10^5\times(P_{ef.}/R^2)\times T(T \geq 3MeV)$$
$$H_x \approx 2.0\times10^5\times(P_{ef.}/R^2)\times T^2(T < 3MeV) \qquad (4)$$

where H_x is the photon dose in mrem/J, $P_{ef.}$ is the laser energy to electron energy conversion efficiency, R is the distance from the target to the measurement point in cm, and T is the hot electron temperature in MeV.

The X-ray dose calculated using Equation 4 at a distance of 1 m is plotted as a function of the normalized laser intensity in Figure 3 (line with circle points). In this calculation, as mentioned before, a laser-to-electron energy conversion efficiency of 30% for laser intensity below 10^{19} W/cm^2 and 50% above 10^{19} W/cm^2 was used. Equation 1 was used to estimate the electron temperature when $I\lambda^2 < 1.6\text{x}10^{17}$ W/cm^{2}μm^2, while Equation 2 was used to estimate the electron temperature when $I\lambda^2 \geq 1.6\text{x}10^{17}$ W/cm^{2}μm^2.

3.3 X-ray dose estimation with 5 mm glass shielding

Because the radiation hazard comes from a laser-target interaction in vacuum, 5-mm-thick glass view port for the target chamber was used to calculate the minimum shielding effect. The material of the glass was assumed as Borosilicate (Pyrex) with a density of 2.23 g/cm^3.

Calculations using the FLUKA Monte Carlo code [35, 36] were conducted to estimate the shielding attenuation for X-ray spectra at various electron temperatures. Equation 3 was used to describe the X-ray source spectrum and a FLUKA source routine was written to sample the Equation 3. The attenuation factor of 5-mm-thick glass shielding for ambient dose equivalent was calculated at different laser intensities.

The X-ray doses with and without the 5-mm-thick glass shielding are summarized in Figure 3, which shows large attenuation from the glass shielding at low intensities due to the low electron temperatures. When the laser intensity gets higher, the attenuation becomes less because the electron temperature gets higher and then the X-ray spectrum gets harder and more difficult to attenuate.

Table 1 gives dose estimates for several different laser system parameters. The dose estimates have an estimated uncertainty factor of ~5, depending on configuration details and system parameters for laser and target. For the MECI laser system with pulse energy of 0.15 J and laser intensity of 2.4x10^{18} W/cm^2, the estimated dose at 1 m is 0.035 mrem/shot and 1250 mrem/hr at 10 Hz.

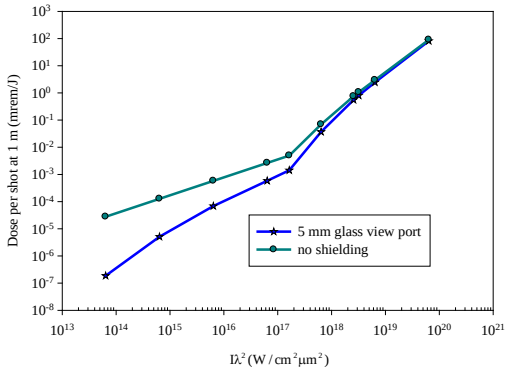

Figure 3. Comparison between the dose per shot at 1 m with and without 5 mm glass view port shielding.

Table 1. Dose estimates (with 5 mm glass shielding) for different TiS laser system parameters. A pulse width of 35 fs is assumed.

Laser System	Repetition rate (Hz)	Pulse Energy (mJ)	Spot size (μm)	T (keV)	Dose rate at 1m (mrem/h)
TiS Regen	1000	3.5	10	18	5.6
TiS MPA	120	20	10	41	32
TiS MPA - MECI	10	150	10	233	1250

3.4 Additional shielding effects

The MECI experiment resides in an X-ray hutch with the following shielding features: a 10.16-cm-thick (4") concrete roof, 0.79-mm-thick (1/32") lead hutch wall, and 1.21-mm-thick stainless steel roll-up door. FLUKA was used to calculate attenuation factors of ambient dose equivalent for these shielding items for low laser intensities of 10^{17}, $5x10^{17}$ and 10^{18} W/cm^2. The X-ray source was assumed to be isotropic and Equation 3 was used to sample the X-ray source spectrum. 5-mm-thick glass shielding was assumed at 1 m from the source before the other hutch shielding materials (5 m away). Therefore, the attenuation factor calculated for hutch shielding is for the X-ray spectrum already hardened by 5mm-thick glass. The calculated attenuation results are shown in Figure 4.

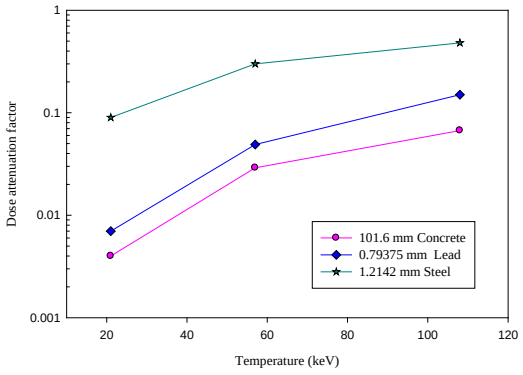

Figure 4. Dose attenuation factors as a function of electron temperature for three hutch shielding materials

Attenuation factors for these shielding items are taken into account for the dose estimation outside the hutch, which affects the hazard control and mitigation as described in Section 5.

4. Other factors affecting the radiation source terms

Two important factors that will affect the radiation outputs are discussed in this section: laser pre-pulse effects and the use of a non-solid target.

4.1 Pre-pulse

Experiment has shown that a laser pre-pulse can increase both the electron temperature and yield significantly. One experiment measured the electron spectra at a laser intensity of 5 x10^{19} W/cm^2 with three pre-pulse levels of 0.01, 0.04 and 0.84 J [29]. It shows that the electron spectrum becomes harder (larger high energy component) with a larger pre-pulse energy. The electron temperature for high-energy hot electrons becomes 5, 8.6 and 16 MeV with a 0.01-J, 0.04-J and 0.84-J pre-pulse, while the hot electron temperature is estimated as ~1 MeV without a pre-pulse based on Figure 2. At the same time the hot electron yield also increases significantly. Since a pre-pulse can make the electron spectrum harder and increase the yield, it can potentially increase the dose level.

4.2 Non-solid targets

In a gas target, the plasma wakefield acceleration mechanism is capable of accelerating electrons to very high energy in a small region, as demonstrated by experiments [37, 38]. Formulas to describe scaling laws for the maximum electron energy can be found in the literature [39]. Several mechanisms limit the energy gain in laser-plasma acceleration: laser diffraction, electron dephasing, pump depletion, and laser-plasma instabilities. The maximum electron energy gain depends on several system parameters. The maximum energy gain is lowest if the acceleration distance is limited by diffraction; this is the most likely scenario if the system is not designed for laser-plasma acceleration [40], which is the case for MECI.

Assuming a gas target with a plasma density of 10^{19} cm^{-3}, the maximum electron energy is estimated as 163 MeV for a laser intensity of $4x10^{18}$ W/cm^2 and 1.15 GeV for 10^{20} W/cm^2. For the gas target case, the laser to electron conversion efficiency is only up to about 1% [41], and, therefore, the electron yield can be estimated as $5.8x10^7$ electrons/pulse and $2.2x10^8$ electrons/pulse at laser intensity of $4x10^{18}$ W/cm^2 and

10^{20} W/cm^2, respectively, assuming all the electrons in one pulse achieve the highest endpoint energy. These estimations for the hazard from gas targets are very crude, but it illustrates the potential magnitudes of the hazard and the need of controls of non-solid targets at these high intensities [42].

5. Mitigation of laser-induced radiation hazard

A graded approach is proposed to mitigate the laser-induced X-ray hazard. Requirements for engineered and administrative controls are based on dose rate and annual dose criteria. The MECI laser system is used as an example to describe this approach. The approach used assumes there is access to the hutch during laser-target operations. Consideration should be given, however, to eliminate the hazard inside the hutch by preventing access during high intensity laser-target operations.

5.1 Safety Envelope, Operation Envelope and Configuration Control

The Safety Envelope (SE) describes achievable laser and target system parameters that result in the maximum credible dose rate. The SE should be used to determine the radiation safety system requirements, unless an Operation Envelope (OE) is established which limits some of the system parameters to lower the maximum dose rate. OE parameters should be controlled by engineered and administrative means such as limiters for laser energy or repetition rate, control of focus spot size, laser shutters, etc.

The SE for MECI laser operations on targets assumes the following parameters:

- Maximum energy per pulse = 150 mJ,
- Minimum pulse length = 40 fs,
- Minimum spot size ($1/e^2$ radius) = 10 μm,
- Maximum repetition rate = 10 Hz.

The corresponding laser peak intensity is 2.4×10^{18} W/cm^2. The maximum occupancy time each year in areas with X-ray hazard is assumed to be 1000 hours. As noted in Table 1, MECI operation at the SE limit gives an estimated dose rate of 1250 mrem/hr at a distance 1 meter from the target (and after 5 mm glass shielding).

A Configuration Control program is needed to ensure that the system capabilities and radiation safety controls are not changed or affected without approval. This program can include elements such as a *Laser Beam Authorization* document and *Laser and Target System Configuration Checklists*.

5.2 Graded approach for hazard controls

To determine the hazard controls requirements, we consider potential radiological doses to two classes of personnel and in two locations. At SLAC, GERT personnel have General Employee Radiological Training and may not receive more than 100 mrem/yr for all SLAC work, while RWT personnel have Radiological Worker Training and cannot receive more than 360 mrem/yr. For MECI laser-target operations, it is proposed that GERT personnel receive no more than 50 mrem/yr and RWT personnel receive no more than 150mrem/yr. The two locations considered are: i) inside the hutch at 1-meter distance from the target, with 5 mm glass viewport shielding, and ii) outside the hutch at 5-meter distance from the target, with shielding from a 5-mm glass viewport and the 1.2 mm steel door.

Because the SE for MECI laser-target operations has such a high potential dose rate, a redundant set of Beam Shut Off Ion Chambers (BSOICs) is needed to detect and terminate high dose rates and to limit the integral dose. The BSOICs will be interlocked with laser operations on target. They are required for all OEs, but the trip points will depend on which OE is approved. They should be placed close to the target chamber at locations that can be most sensitive to detect ionizing radiation. The BSOICs should be sensitive enough to detect the natural background level of 10 μrem/h.

For MECI operation, four different OEs (A, B, C and D) are proposed with different levels of potential dose rate. These OEs are shown in Figure 5 as a function of pulse energy and the quantity $I\lambda^2$. Each OE has associated requirements for engineered and administrative controls, with OE level C having the most stringent requirements. The proposed controls are set in a graded approach commensurate with the level of the radiological hazard.

If OE level A is approved for MECI operation with 150 mJ pulse energy and 10 Hz operation, then the peak intensity must be restricted to not exceed 3×10^{15} W/cm^2. The only required engineered controls would be those for configuration control to stay within the OE limit on peak intensity and the BSOICs mentioned above. Administrative controls would include GERT training for unescorted entry to the MECI experimental hutch, and posting of the hutch as a controlled area with a GERT requirement.

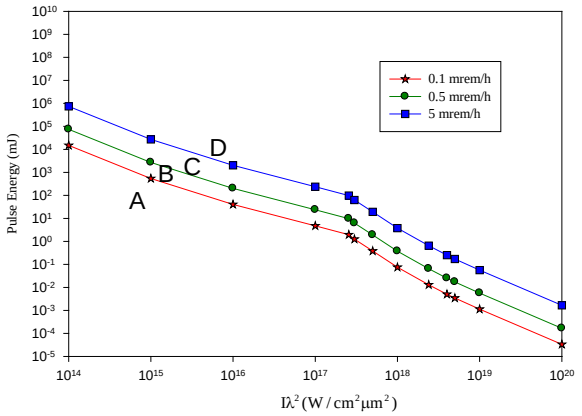

Figure 5. Four zones of radiation levels at different combinations of laser intensity and pulse energy (dose rate are at 1 m outside 5 mm glass shielding; a repetition rate of 10 Hz is assumed).

If OE Level B is approved for MECI operation with 150 mJ pulse energy and 10 Hz operation, then higher peak intensities up to 1.5×10^{16} W/cm^2 would be permitted. Administrative controls would include GERT training for unescorted entry to the MECI experimental hutch, and posting of the hutch as a Radiologically Controlled Area (RCA) with a GERT requirement.

If OE Level C is approved for MECI operation with 150 mJ pulse energy and 10 Hz operation, then a peak intensities up to 1.6×10^{17} W/cm^2 would be permitted. The hutch would be posted as a Radiologically Controlled Area (RCA) with access limited to RWT personnel carrying a personnel dosimeter. Note that at a dose rate of 5 mrem/h at 1 m, the 150 mrem/y dose level for personnel inside the hutch corresponds to 30 hours of laser-on-target operation. Therefore, OE Level C requires additional engineered and/or administrative measures to ensure that RWT personnel who access the hutch do not exceed their annual dose limit.

OE Level D (shown in Figure 5) has potential dose rates exceeding 5 mrem/hr. The SE for MECI is in this region but is not yet considered for MECI operation approval. Such approval would require additional controls, which might include not permitting personnel access to the hutch during laser-target operations, and may also require additional shielding.

The four OE regions shown in Figure 5 can be used to evaluate potential radiation hazards for a wide range of laser systems. A repetition rate of 10 Hz is assumed to generate this figure, but since dose rate is proportional to repetition rate the results can be easily scaled. Once the OE region is established for a given laser system, the corresponding radiation controls to mitigate the hazard can be determined.

Summary

We have presented preliminary analysis results for X-ray radiation hazards from laser-target interactions at laser intensities between 10^{14} and 10^{20} W/cm^2. The radiation source term depends on the laser-to-electron conversion efficiency, the hot electron energy spectrum and effective temperature, and the X-ray spectrum and dose due to bremsstrahlung. Estimated dose rates are given which have an associated uncertainty factor of ~5.

The electron and X-ray energy spectrum is an exponentially decreasing curve characterized by an electron temperature, which can be estimated with two analytic formulas at low and high laser intensities. The X-ray dose, in mrem/J, was estimated using analytic equations that are based on a combination of theory and experiment. Shielding calculations for ambient dose equivalent were performed using the FLUKA Monte Carlo code. Semi-quantitative effects from laser pre-pulse and non-solid targets were also discussed.

Based on the dose estimation, a preliminary graded approach with a combination of engineered and administrative controls is proposed to mitigate and control the laser induced X-ray hazard.

Acknowledgements

We would like to express our appreciation to Greg Hays, Hae Ja Lee, Richard M. Boyce and Bob Nagler (SLAC) for useful discussions and providing related information on MECI parameters; and Hui Chen and Scott Wilks (LLNL) for providing information about the electron temperature study results.

This work is supported by the U.S. Department of Energy under contract number DE-AC02-76SF00515.

References

[1] S. C. Wilks and W. L. Kruer, IEEE J. Quantum Electron. 33 (1997) 1954.

[2] H.A. Baldis, E.M. Campbell, W.L. Kruer. Handbook of Plasma Physics, Chapter 9, Elsevier Science Publishers, (1991).

[3] L. M. Chen et al., Study of hard x-ray emission from intense femtosecond Ti: sapphire laser-solid ,11 (2004) 4439.

[4] T. Guo et al., Generation of hard x-rays by ultrafast terawatt lasers, Rev. Sci. Instr., 72 (2001) 41.

[5] H.A. Baldis, E.M. Campbell, W.L. Kruer. Handbook of Plasma Physics, Chapter 9, Elsevier Science Publishers, (1991).

[6] L. M. Chen et al., Study of hard x-ray emission from intense femtosecond Ti: sapphire laser-solid ,11 (2004) 4439.

[7] T. Guo et al., Generation of hard x-rays by ultrafast terawatt lasers, Rev. Sci. Instr., 72 (2001) 41.

[8] F. Borne, D. Delacroix, J. M. Gele, ea al. Radiation Protection Dosimetry 1 (2002) 61.

[9] Fuchs, J., Antici, P., D'Humieres, E., Lefebvre, E., Borghesi, M., Brambrink, E., Cecchetti, C. A.,Kaluza, M., Malka, V., Manclossi, M., Meyroneinc, S., Mora, P., Schreiber, J., Toncian, T., Pepin, H. & Audebert, R. Laser-driven proton scaling laws and new paths towards energy increase. Nature Phys., 2, 1, (Jan) (2006) 48.

[10] R J Clarke, D Neely, R D Edwards. J. Radiol. Prot. 26 (2006) 277.

[11] Y. Hayashi , A. Fukumi et al. Radiat Prot Dosimetry 121 (2) (2006) 99.

[12] Brunel.F. Not-so-resonant, resonant absorption. Phys. Rev. Lett. 59, 52–55 (1987).

[13] Kruer, W. L. and Estabrook, K. JxB heating by very intense laser light. Phys. Fluids. 28, 430–432(1985).

[14] Esarey, E. Sprangle, P. and Senior Member. Overview of plasma-based accelerator concepts. IEEE Trans. Plasma Sci. 24, 252–288 (1996).

[15] G. Hays, B. White, H. J. Lee, D. Marsh, R. M. Boyce, J. Galayda. Physics Requirements for the MECI Laser Systems, LCLS RPD SP-391-001-05 R1 (2009).

[16]https://slacportal.slac.stanford.edu/sites/lcls_public/instruments/mec/Pages/default.aspx

[17] S. P. Hatchett et al., Phys. Plasmas 7 (2000) 2076.

[18] M. H. Key et al., Phys. Plasmas 5 (1998) 1966.

[19] W. Theobald et al., Phys. Plasmas 13, 043102 (2006).

[20] J. Myatt et al., Phys. Plasmas 14, 056301 (2007).

[21] Y. Ping et al., Phys. Rev. Lett. 100, 085004 (2008).

[22] Yasuike, K., Key, M. H., Hatchett, S. P., Snavely, R. A., and Wharton, K. B. Rev. Sci. Instrum. 72, (2001) 1236.

[23] Hesham Khater, Sandra Brereton et.al. Shielding analysis for X-ray sources generated in target chamber of the national ignition facility. Nuclear Technology. (2009) 381.

[24] Stephen P. Hatchett, Curtis G. Brown, Thomas E. Cowan et al. Electron, photon, and ion beams from the relativistic interaction of Petawatt laser pulses with solid targets, Phys. Plasmas (2000) 2076.

[25] Private communication with Hui Chen and Scott Wilks (2010).

[26] Private communication with Hesham Khater (2010).

[27] M. D. Perry, J. Sefcik, T. Cowan, S. Hatchett, et al. Laser driven radiography, UCRL-ID-129314, LLNL, (1997).

[28] K. W. D. Ledingham, I. Spencer, T. McCanny et,al. Photonuclear Physics when a Multiterawatt Laser Pulse Interacts with Solid Targets. Phys. Rev. Lett. 84 (2000) 899.

[29] Hui Chen et al. Escaping Hot Electron Measurements from Small to Large Short Pulse Laser Facilities,LLNL-PRES-416551 (2009).

[30] D. D. Meyerhofer, H. Chen, J. A. Delettrez, B. Soom, S. Uchida, and B. Yaakobi, Phys. Fluids B. (1993) 2584.

[31] Hui Chen et al. Physics of plasmas, 16, 020705 (2009) .

[32] Y. Ping et al., Phys. Rev. Lett. 100, 085004 (2008).

[33] Bob Nagler, Estimate of the X-ray spectrum produced by MEC laser systems, internal communication, (2009).

[34] Swanson, W. P. Radiological safety aspects of the operation of electron linear accelerators. IAEA Technical Report Series 188 (IAEA, P.O. Box 100, Wagramer Strasse 5, A-1400 Vienna, Austria) (1979).

[35] G. Battistoni, S. Muraro, P.R. Sala, F. Cerutti, A. Ferrari, S. Roesler, A. Fassò, The FLUKA code: Description and benchmarking, *Proceedings of the Hadronic Shower Simulation Workshop 2006,* Fermilab 6-8

September 2006, M. Albrow, R. Raja eds., AIP Conference Proceedings 896, 31 (2007).
[36] A. Fassò, A. Ferrari, J. Ranft and P. R. Sala, FLUKA a multi-particle transport code. CERN-2005-10, INFN/TC_05/11, SLAC-R773 (2005).
[37] Leemans et al. GeV electron beams from a centimetre-scale accelerator. Nature Physics 418 (2006) 696.
[38] Blumenfeld et al. Energy doubling of 42 GeV electrons in a metre-scale plasma wakefield accelerator. Nature 445 (2007) 741.
[39] E. Esarey, C. B. Schroeder, and W. P. Leemans. Physics of laser-driven plasma-based electron accelerators. Reviws of Modern Physics,81 (2009).
[40] Eric Colby and Mark Hogan, private communication (2009).
[41] W. P. Leemans, private communication (2010).
[42] Rick Donahue, private communication (2010).

Meet the Authors

Rui Qiu is a visiting Health Physicist with the Radiation Protection Department at SLAC. She obtained her Bachelor's degree from Tsinghua University in China in 2002 in Nuclear Science and Technology and received her Doctorate in Health Physics also from Tsinghua University in 2007. From October 2006 to October 2007, she worked as a researcher at Radiation Safety Division of Pohang Accelerator Laboratory in Korea. Her research interests cover various aspects in the Monte Carlo method, radiation dosimetry, radiation effect, and radiation protection.

James Liu is the radiation physics team lead for LCLS photon instruments and for SSRL at SLAC. He also serves as the Dosimetry and Radiological Environmental Protection Group Leader. He is a Certified Health Physicist with a Ph.D. in Health Physics from Texas A&M University. He has spent over 20 years in the support for the radiological design and operations of particle accelerators at SLAC, as well as R&D in health physics areas.

Alyssa Prinz is a radiation physicist for LCLS photon instruments and for SSRL at SLAC. She has a Ph.D. in Particle Physics from Stanford University. She has spent ~10 years in the support for the radiological design and operations of particle accelerators at SLAC.

Sayed Rokni is the Radiation Safety Officer and the Radiation Protection Department Head at SLAC. He is a Certified Health Physicist with a Ph.D. in Nuclear Physics from Utah State University. He has spent 23 years in research in radiation measurements and in design and development of shielding and safety systems for protection against ionizing radiation in accelerators.

Michael Woods, CLSO, is the Laser Safety Officer at SLAC. He is an Engineering Physicist, with a B.Sc. in Engineering Physics from Queen's University in Kingston, Ontario, Canada and a Ph.D. in High Energy Physics from the University of Chicago. He has spent 15 years as a researcher in experimental particle physics and accelerator physics utilizing high power laser systems. He became SLAC LSO in 2008.

Zhenghua Xia is a Radiation Physicist at SLAC. She received a B.Eng. degree in Nuclear Engineering from Tsinghua University, China in 2001. She has a Masters degree in Health Physics from University of Cincinnati, OH and a Ph.D. in Heath Physics from Texas A&M University. Prior to her job at SLAC, she worked as a health physicist and dosimetrist in LANDAUER INC company.